

The measurement-induced phase transition in strongly disordered spin chains

Yicheng Tang,¹ Pradip Kattel,^{1,2} Arijeet Pal,³ Emil A. Yuzbashyan,¹ and J. H. Pixley^{1,4}

¹*Department of Physics and Astronomy, Center for Materials Theory,
Rutgers University, Piscataway, NJ 08854, United States of America*

²*Department of Quantum Matter Physics, University of Geneva,
Quai Ernest-Ansermet 24, 1211 Geneva, Switzerland*

³*Department of Physics and Astronomy, University College London,
Gower Street, London WC1E 6BT, United Kingdom*

⁴*Center for Computational Quantum Physics, Flatiron Institute, 162 5th Avenue, New York, NY 10010*

We investigate the dynamics of strongly disordered spin chains in the presence of random local measurements. By studying the transverse-field Ising model with a site-dependent random longitudinal field and an effective l -bit many-body localized Hamiltonian, we show that the prethermal and MBL regimes are unstable to local measurements along any direction. Any non-zero measurement density induces a volume-law entangled phase with a subsequent phase transition into an area-law state as the measurement rate is further increased. The critical measurement rate p_c , where the transition occurs, is exponentially small in the strength of disorder W and the average overlap between the measurement operator and the local integrals of motion O as $p_c \sim \exp[-\alpha W/(1 - O^2)]$. In the measurement-induced volume-law phase, the saturation time scales as $t_s \sim L$, contrasting the exponentially slow saturation $t_s \sim e^{aL}$ in the prethermal and MBL regimes at $p = 0$.

Localization of quantum particles has remained of central interest in condensed matter physics [1, 2]. While it is well known that strong disorder localizes noninteracting fermions [3, 4], the role of interactions in many-body localization (MBL) at finite energy density is a subtle and challenging question [5–10]. The prethermal regime preceding the MBL phase exhibits dynamical properties resembling full MBL [11–13], for small system sizes, in classical and quantum simulations [14–16]. The instability of the MBL regime to quantum measurements can provide a new perspective on localization, as random local measurements induce a form of dynamical localization through wavefunction collapse, which is distinct from quantum interference. In d -dimensional monitored free-fermionic circuits, this interplay has been made explicit by mapping the system to $d + 1$ -dimensional free fermions in quenched disorder; the Anderson localized phase in $d + 1$ now corresponds to an area-law scaling of the entanglement entropy [17–20]. However, in the presence of strong interactions, this mapping no longer applies, and the interplay of disorder, interactions, and measurements offers a versatile setting to explore new dynamical effects and phase transitions.

Surprisingly, in the presence of interactions, localization induced by static disorder and measurement are, in fact, directly competing as they correspond to different forms of localized behavior. This is due to the physical spin operators having finite support over many l -bits, each projective measurement acts as a non-commuting perturbation on an extended set of integrals of motion. Repeated measurements, therefore, continually scramble the l -bit degrees of freedom and destabilize the MBL structure, even when the overlap with a single l -bit is exponentially small, which was studied by analogous stabilizer circuits mapped to measurement-only models [21].

At sufficiently high measurement rates (in particular directions), the MBL model has been found to undergo a measurement-induced phase transition (MIPT) into an area-law phase, which is unrelated to the underlying MBL phase. In contrast, the volume-law phase ceases to exist for measurements of the exact l -bit operator [22], which are still exponentially complex to construct. In practice, only physical spins, which have partial overlaps with l -bits, are measurable, as depicted in Fig. 1(a). This deviation plays a crucial non-perturbative role in the instability of MBL dynamics to measurements. A precise understanding of how measurements impact the stability of the prethermal and MBL regimes has been lacking and is crucial for a comprehensive picture of the instabilities of MBL in open system dynamics. In particular, prior work [22–24] concluded that if you measure physical operators that “align” strongly with the l -bit operators then there is no volume law phase. However, we show that this conclusion is incorrect and provide strong numerical evidence of a non-zero critical measurement rate that follows a universal form for any measurement direction that is albeit exponentially small in the disorder strength, thus demonstrating the instability of the MBL phase to random local measurements.

In this work, we investigate the monitored quantum dynamics of strongly disordered spin-1/2 chains without any space-time symmetries other than the energy conservation. We consider their unitary Hamiltonian dynamics interspersed by random local measurements along an arbitrary direction denoted by the angle θ , see Fig. 1. To compute the dynamics, we utilize a Chebyshev expansion of the unitary time evolution operator [25], which allows an efficient and accurate truncation. As a result, we achieve system sizes comparable to those of quantum circuit simulations, which help us to determine the phase

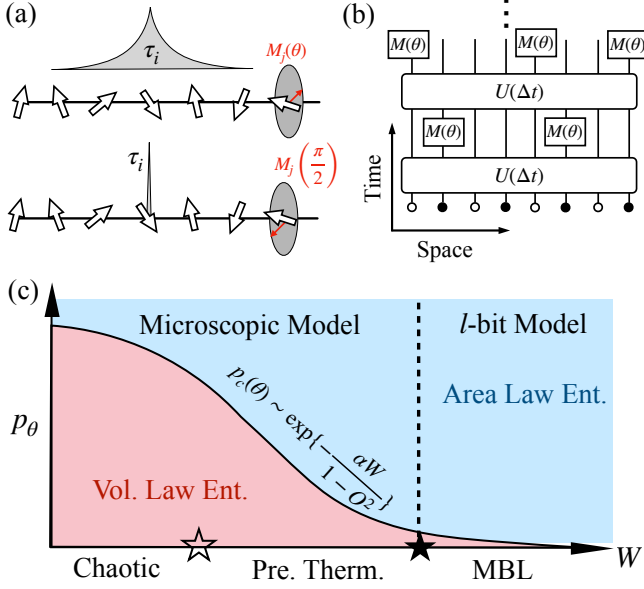


FIG. 1: (a) The top panel is a schematic of the typical support of an l -bit operator, localized at site i in the microscopic model, with each qubit measured randomly with $M_i(\theta)$ in the $x-z$ plane. The bottom panel shows a schematic of the l -bit operator in the l -bit model, with each qubit measured randomly in the x direction. (b) Illustration of measurement protocol with unitary Hamiltonian dynamics $U(\Delta t)$ followed by random measurements $M_i(\theta)$ with rate p . (c) Illustration of the phase diagram for the MBL system with measurement in the space of disorder strength W and measurement rate p_θ at angle θ . For any θ , the critical measurement rate $p_c \sim \exp\{-\frac{\alpha W}{1-O^2}\}$ for large W labels the boundary between volume and area-law entangled phases with O being the overlap between the measurement operator (defined explicitly for in Eq. (6)).

boundary separating volume-law and area-law entangled phases.

We show that the boundary is exponentially small in both the disorder strength and the overlap of local measurement operators with the l -bit degrees of freedom. We complement this analysis with a study of the saturation time scales in the l -bit limit of the model, which shows that the $p > 0$ region of the phase diagram, where this scale grows linearly with the system size, is not smoothly connected to the $p = 0$ line, where it is exponentially slow. These results are supported by both the spin-chain model in the prethermal MBL regime and the l -bit Hamiltonian, suggesting that they are generic, and can be tested on current quantum platforms such as trapped-ion and superconducting-qubit experiments that have realized MBL [26–35] and MIPTs [36–40].

To study the interplay of measurements and MBL, we

focus on a repeated two-stage protocol, which consists of alternating unitary evolution and projective measurements as shown in Fig. 1(b). In the unitary step, the system evolves under the unitary operator that we take to be the same each time it is applied (i.e., it is a Floquet operator) $U = e^{-iH\Delta t}$, and we set $\Delta t = 1/J$ throughout. We consider two different Hamiltonians in this work: the microscopic Hamiltonian (1) and the l -bit Hamiltonian (2).

The microscopic Hamiltonian that we analyze is the disordered transverse-field Ising model with a site-dependent random longitudinal field

$$H(W, \{\eta\}) = J \sum_{i=1}^L (\sigma_i^z \sigma_{i+1}^z + \sigma_i^x + W \eta_i \sigma_i^z). \quad (1)$$

The strength of disorder is denoted W , and η_i are random variables at each site that are drawn from the uniform distribution between $[-1, 1]$. To ascertain the small- L behavior of this Hamiltonian, we analyze its level spacing ratio using exact diagonalization and present the results in End matter. We observe a clear transition from Wigner-Dyson to Poisson-like behavior as the disorder is increased, with a crossing that drifts up to $W \gtrsim 3.2$, which has been interpreted as the onset of MBL in small systems. However, recent studies suggest that true many-body localization may only occur for significantly stronger disorder strengths in the thermodynamic limit [12, 41, 42]. In the intermediate prethermal regime $W \gtrsim 3.2$, the system displays slow entanglement dynamics and suppressed thermalization, which is the parameter regime of the microscopic model we focus on in this work.

In addition to analyzing the prethermal regime of this finite system size MBL model, we also investigate another Hamiltonian (the l -bit Hamiltonian), which is by construction in the MBL phase. When the system is in the MBL phase, there exists a complete set of emergent local integrals of motion, illustrated in Fig. 1(a). Therefore, to study the effects of measurement in the MBL phase, we consider an effective MBL Hamiltonian in the l -bit (τ) basis [43, 44], which is related to the physical σ basis by a local unitary transformation. In this basis, the diagonal form of the MBL Hamiltonian is

$$H_{l\text{-bits}}(\{\eta\}) = \sum_i h \eta_i \tau_i^z + \sum_{i,j} \eta_{ij} e^{-m|i-j|} \tau_i^z \tau_j^z + \dots \quad (2)$$

where \dots stands for the higher order terms in terms of the l -bits, $\eta \in [0, 1]$ is a random variable. In the following, unless otherwise specified, we drop the higher-order terms and choose $h = 5$ for the l -bit model. Without measurement, $p = 0$, the Hamiltonian dynamics generates entanglement entropy with a logarithmic growth $S(t) \sim \ln t$ characteristic of MBL systems [15, 16, 45] for both the microscopic Hamiltonian (1) and the l -bit Hamiltonian (2).

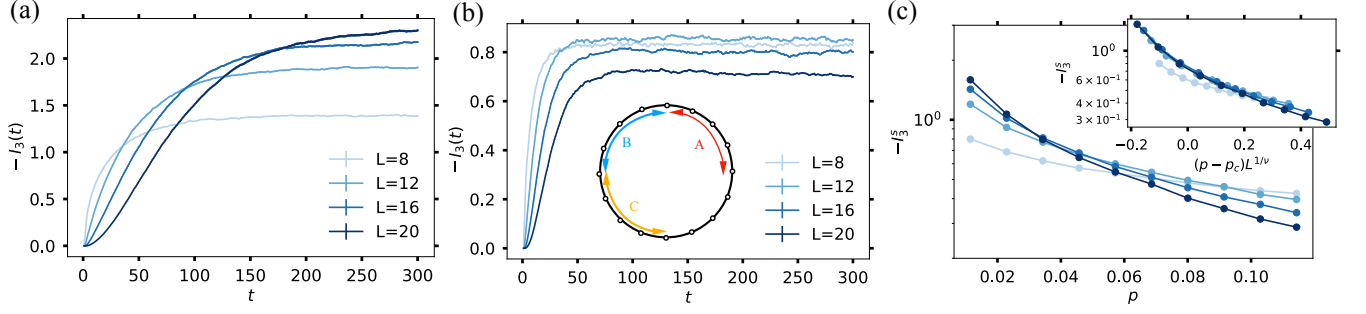


FIG. 2: Tripartite mutual information $I_3(t)$ for the evolution under Hamiltonian (1) and random measurements for measurement angle $\theta = \frac{\pi}{2}$ and various system sizes L . The disorder strength is $W = 5$ and the measurement probability is $p = 0.01$ in (a) and $p = 0.09$ in (b) corresponding to the volume-law and the area-law entangled phases, respectively. The inset in (b) depicts the geometry used to compute $I_3(t)$. (c) Tripartite mutual information in the steady state I_3^s as a function of p with a critical value $p_c \simeq 0.039$. The inset shows the data collapse for the microscopic model using the critical exponent $\nu \simeq 1.6$ extrapolated from the l -bit model.

In the measurement step, we perform a projective measurement with probability p at each site. We measure in the xz plane at site i the operator

$$M_i(\theta) = \cos \theta \sigma_i^z + \sin \theta \sigma_i^x, \quad (3)$$

which interpolates between $\sigma_i^z = M_i(0)$ and $\sigma_i^x = M_i(\frac{\pi}{2})$ and has measurement outcome $m_i = \pm 1$. This measurement consists of the projectors $P_{m_i}(\theta) = (1 \pm M_i(\theta))/2$ with eigenvalues $m_i = \pm 1$ and the state transforms according to

$$|\psi\rangle \rightarrow \frac{1}{p_{m_i}} P_{m_i}(\theta) |\psi\rangle, \quad (4)$$

with Born probability $p_{m_i} = \langle \psi | P_{m_i}(\theta) | \psi \rangle$ up to normalization. As a result, the time evolution is non-unitary, and the state is now indexed by the measurement history labeled by the set $\{m_k\}$. Notice that purely τ^z measurements in the l -bit model commute with the Hamiltonian and produce a steady state that is a product state for any finite measurement rate. Therefore, only measurements with a finite τ_x component lead to nontrivial dynamics.

Combining the unitary dynamics with the above measurement protocol, we evolve the system by iterating these two steps as shown in Fig. 1(b), starting from a random product state $|\psi_0\rangle = \otimes_{i=1}^L |\theta_i, \phi_i\rangle$ where each qubit is initialized in a pure state parameterized by spherical angles θ_i and ϕ_i as $|\theta, \phi\rangle = (\cos \frac{\theta}{2}, e^{i\phi} \sin \frac{\theta}{2})$. At every time step t , we first evolve the state $|\psi(t)\rangle$ as $|\psi(t + \frac{1}{2})\rangle = e^{-iH(\{\eta\})\Delta t} |\psi(t)\rangle$. To simulate the time evolution of the system under Hamiltonian dynamics, we approximate the unitary time-evolution operator with a Chebyshev polynomial expansion, as discussed in End matter. A benefit of the Hamiltonian acting over a short time for each step of the evolution is that it allows us to truncate the Chebyshev expansion at a low order. After

the unitary evolution, the measurement step is applied, $|\psi(t + 1)\rangle = \prod_{\{m_i\}} \frac{1}{p_{m_i}} P_{m_i} |\psi(t + \frac{1}{2})\rangle$ with a set of measurement outcomes $m_i(t)$ if the i -th qubit is measured. The resulting state at time t depends on the random variable $\{\eta\}$ and measurement outcomes $\{m_i(t)\}$, and we label it as $|\psi(t)\rangle_{\{\eta, m_i(t)\}}$.

At each step t , we compute the tripartite mutual information for the state $|\psi(t)\rangle_{\{\eta, m_i(t)\}}$ defined as $I_3^{\{\eta, m_i(t)\}}(t) = S_A + S_B + S_C + S_{ABC} - S_{AB} - S_{BC} - S_{AC}$, where $S_X = -\rho_X \ln \rho_X$ is the von-Neumann entropy of subsystem X with reduced density matrix $\rho_X = \text{Tr}_{\bar{X}} (|\psi(t)\rangle_{\{\eta, m_i(t)\}} \langle \psi(t)|_{\{\eta, m_i(t)\}})$. The subsystems A , B , and C are shown in Fig. 2(b); each corresponds to one quarter of the system. We average the mutual information over 2000 samples of random parameters $\{\eta\}$ and quantum trajectories $\{m_i(t)\}$, $I_3(t) = [\bar{I}_3^{\{\eta, m_i(t)\}}(t)]$, with \bar{X} indicating the average of X over random parameters $\{\eta\}$ and $[X]$ indicating the average over the quantum trajectory $\{m_i(t)\}$. In Fig. 2 (a) and (b), we present two representative examples of the time evolution of $I_3(t)$ with parameters $W = 5$ and $\theta = \frac{\pi}{2}$, differing only in the value of the measurement rate p . Both show saturation to a steady-state value $I_3^s = I_3(t \rightarrow \infty)$ under the repeated measurement protocol.

To probe the entanglement structure of the steady state, we analyze the scaling of the steady state tripartite mutual information I_3^s as a function of the system size L and measurement rate p at a fixed measurement angle $\theta = \pi/2$ and randomness $W = 5$, see Fig. 2 (c). A transition between volume-law and area-law entanglement is detected from the crossing of the $I_3^s(p)$ curves for different system sizes L , which determines the critical measurement rate p_c . Near the critical point in the long time limit, the tripartite mutual information follows

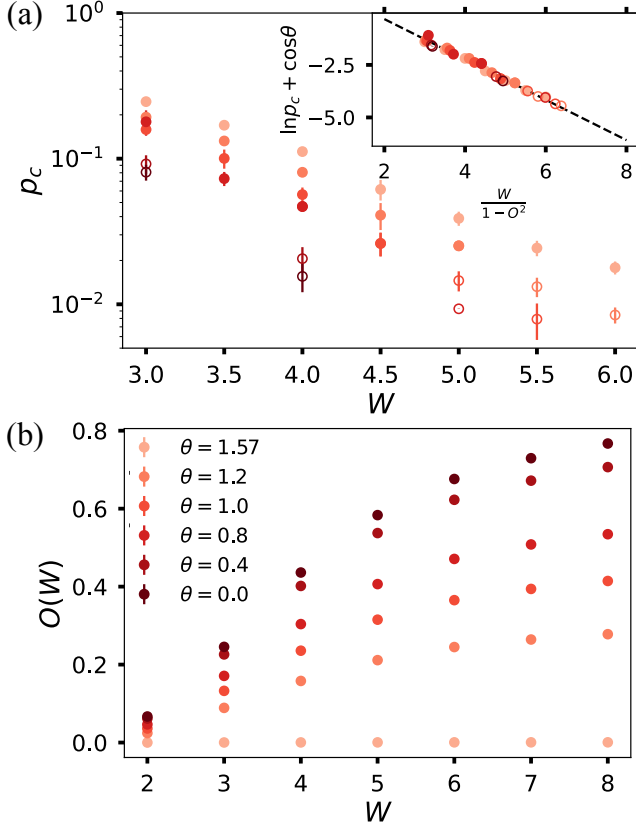


FIG. 3: (a) The W - and θ -dependence of the critical measurement rate $p_c(W, \theta)$ defines the phase boundary between volume-law entanglement, $p < p_c$, and area-law entanglement, $p > p_c$, for the model (1). The inset shows the data collapse onto the curve given by Eq. (7). The hollow markers indicate data points where p_c shows a significant finite-size effect. (b) Overlaps between the local integral of motion and the measurement operator $O(\theta, W)$ as defined in Eq. (6) for Hamiltonian (1)

a universal scaling function [46–48]

$$I_3^s = I_3(t \rightarrow \infty) \sim f\left((p - p_c)L^{1/\nu}\right) \quad (5)$$

where ν is the correlation length exponent and $f(x)$ is a smooth function. Because of strong finite-size effects, ν cannot be reliably extracted for the microscopic model. However, the l -bit model yields $\nu = 1.6 \pm 0.01$.

The complete phase diagram is obtained by extracting the critical measurement rate $p_c(\theta, W)$ from the crossings of the $I_3^s(p)$ curves at various values of W and θ . We observe that for large randomness $W \geq 3$, the critical measurement rate is exponentially small $p_c \sim e^{-f(\theta)W}$ as shown in Fig. 3. To determine $f(\theta)$, we compute the overlap between the measurement operator in Eq. (3) and the emergent local integral of motion (per disorder

sample), defined as [49]

$$O(\theta, W) = \frac{1}{2^L} \text{Tr} \left(M(\theta) \bar{L}_i(W, \{\eta\}) \right), \quad (6)$$

where $L_i(W, \{\eta\}) = V^\dagger \text{diag}(V \sigma_i^z V^\dagger) V$ and V is the unitary operator that diagonalizes the Hamiltonian $H(W, \{\eta\})$ and $\text{diag}(A)$ is a diagonal matrix with the same diagonal elements as A . By construction, the local integral of motion $L_i(W, \{\eta\})$ is a conserved charge, $[L_i, H] = 0$, which depends only on the Hamiltonian. The numerical values of $O(\theta, W)$ averaged over 500 samples of random variables η_i are shown in Fig. 3(b).

This overlap characterizes the extent to which measurement “freezes” an integral of motion. We compare the critical measurement rate p_c with the overlap O shown in Fig. 3 with an ansatz

$$p_c(W, \theta) = p_0 \exp \left(-\frac{\alpha W}{1 - O(\theta, W)^2} - \cos \theta \right) \quad (7)$$

where $p_0 = 4.9$ and $\alpha = 0.96$ are obtained by collapsing the data onto a single curve, see the inset in Fig. 3. Eq. (7) implies several key consequences. First, it indicates that there is always a phase transition from volume to area-law entanglement in the prethermal and MBL systems due to measurements for any value of the overlap between the measurement operator and the l -bit degrees of freedom. At the same, the phase boundary out of the volume-law phase is exponentially small as the parameters W and θ are increased. Finally, it also suggests that the prethermal MBL regime is unstable to any non-zero measurement rate in any direction, irrespective of the nature of the l -bit operators. To understand this instability, we now turn to the l -bit model (2).

The l -bit Hamiltonian puts us deep into the MBL phase by construction, and we find that the finite-size effects are significantly suppressed as compared to the microscopic model (2) because the localization length is strictly bounded. This allows us to obtain better numerical results for I_3^s and establish that the τ^x measurements produce an MIPT with $p_c = 0.18$ and the critical exponent $\nu \approx 1.6 \pm 0.01$ as shown in Fig. 4(a). Moreover, the dynamical exponent $z = 1$ as we demonstrate in the End Matter.

In Fig. 4(c), we show that in the presence of measurements, the entanglement entropy grows faster than in the case of purely unitary dynamics destroying the logarithmic growth in the MBL state and indicating that the MBL dynamics is unstable with respect to any non-zero density of local measurements. To study the instability of the MBL phase under measurements, we investigate the system at the saturation time t_s , defined by $I_3(t > t_s) = I_3^s$, see Fig. 4(b). In the MBL phase ($p = 0$), t_s scales exponentially with the system size $t_s \sim e^{aL}$ [15]. However, when a finite density of measurements is present ($p > 0$), the exponentially slow re-

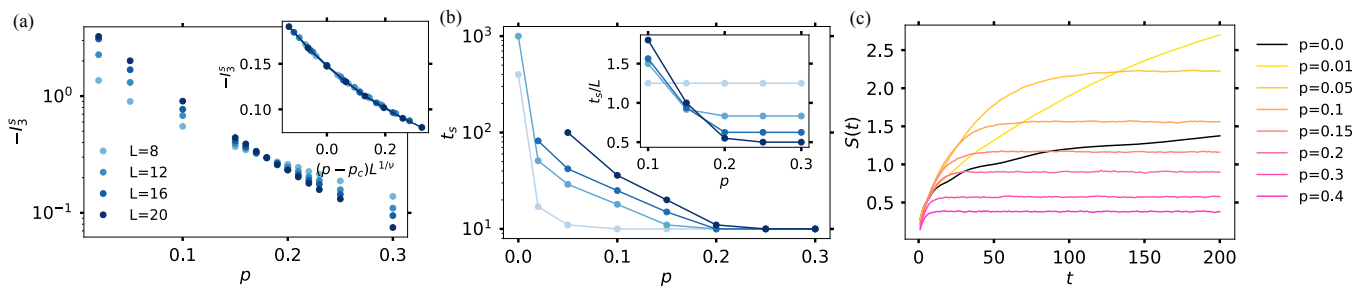


FIG. 4: Entanglement dynamics for the l -bit model (2). (a) Plots of the steady state mutual information I_3^s vs. the measurement rate p for different system sizes L crossing at $p = p_c$. The inset shows the data collapse with the scaling $(p - p_c)L^{1/\nu}$ as defined in Eq. (5), where $\nu \simeq 1.6$. (b) Saturation time t_s (t_s/L in the inset) as a function of p . The t_s/L plots collapse consistent with $t_s \sim \mathcal{O}(L)$ when $p < p_c = 0.18$ and the system is in the volume-law entanglement phase, while the t_s plots collapse for $p > p_c$ when the system is in the area-law entangled phase where $t_s \sim \mathcal{O}(1)$. Legend is shared with (a). (c) Half-cut entanglement entropy for different measurement rates p demonstrating that the entanglement entropy can grow faster with measurements than without.

laxation collapses to a linear scaling $t_s \sim L$ characteristic of a volume-law entangled phase. Throughout the volume-law regime ($0 < p < p_c$) one finds $t_s \propto L$. By contrast, in the area-law phase ($p > p_c$) the saturation time becomes size-independent, $t_s \sim \mathcal{O}(1)$.

We resolve the phase diagram of monitored MBL systems by determining the disorder-dependent critical measurement rate p_c at which the entanglement structure changes qualitatively. Starting from an MBL regime with slow, logarithmic entanglement growth, we find that any nonzero measurement rate immediately produces a stable volume-law phase. Upon further increasing the rate, the system undergoes a sharp transition at a finite $p_c(W, \theta)$ into a measurement-dominated area-law phase, with p_c decreasing exponentially with disorder strength. By mapping $p_c(W, \theta)$ across disorder and measurement angles, we completely determine the boundary between these phases. The resulting transition is a property of the monitored dynamics itself and does not track the underlying unitary MBL crossover, demonstrating that MBL systems, once monitored, generically exhibit a three-stage structure: slow-entangling MBL at $p = 0$, a robust volume-law regime for any $p_c(W, \theta) > p > 0$, and an area-law phase for $p > p_c(W, \theta)$.

Acknowledgement: We thank Anushya Chandran, Vedika Khemani, and Sarang Gopalakrishnan for useful discussions, and we thank David Huse for in-depth discussions. This work is partially supported by the Army Research Office Grant No. W911NF-23-1-0144 (P.K. and J.H.P.) and the Rutgers Samuel Marateck Fellowship (Y.T.). A.P. was funded by the European Research Council (ERC) under the EU's Horizon 2020 research and innovation program (Grant Agreement No. 853368). A.P. thanks the Physics departments at Princeton and Harvard Universities for their support and hospitality during the sabbatical where part of this work was carried out.

-
- [1] E. Abrahams, P. W. Anderson, D. C. Licciardello, and T. V. Ramakrishnan, Scaling theory of localization: Absence of quantum diffusion in two dimensions, *Physical Review Letters* **42**, 673 (1979).
 - [2] F. Alet and N. Laflorencie, Many-body localization: An introduction and selected topics, *Comptes Rendus Physique* **19**, 498 (2018).
 - [3] P. W. Anderson, Absence of diffusion in certain random lattices, *Phys. Rev.* **109**, 1492 (1958).
 - [4] P. Anderson, 50 years of anderson localization, 50 Years Of Anderson Localization. Edited by PW Anderson. Published by World Scientific Publishing Co. Pte. Ltd (2010).
 - [5] V. Oganesyan and D. A. Huse, Localization of interacting fermions at high temperature, *Physical Review B—Condensed Matter and Materials Physics* **75**, 155111 (2007).
 - [6] R. Nandkishore and D. A. Huse, Many-body localization and thermalization in quantum statistical mechanics, *Annu. Rev. Condens. Matter Phys.* **6**, 15 (2015).
 - [7] D. A. Abanin, E. Altman, I. Bloch, and M. Serbyn, Colloquium: Many-body localization, thermalization, and entanglement, *Reviews of Modern Physics* **91**, 021001 (2019).
 - [8] S. D. Geraedts, R. Nandkishore, and N. Regnault, Many-body localization and thermalization: Insights from the entanglement spectrum, *Physical Review B* **93**, 174202 (2016).
 - [9] J. Z. Imbrie, On many-body localization for quantum spin chains, *Journal of Statistical Physics* **163**, 998 (2016).
 - [10] J. Šuntajs, J. Bonča, T. Prosen, and L. Vidmar, Quantum chaos challenges many-body localization, *Physical Review E* **102**, 062144 (2020).
 - [11] W. De Roeck and F. m. c. Huveneers, Stability and instability towards delocalization in many-body localization systems, *Phys. Rev. B* **95**, 155129 (2017).
 - [12] D. M. Long, P. J. Crowley, V. Khemani, and A. Chandran, Phenomenology of the prethermal many-body lo-

- calized regime, *Physical Review Letters* **131**, 106301 (2023).
- [13] D. A. Abanin, W. De Roeck, W. W. Ho, and F. m. c. Huveneers, Effective hamiltonians, prethermalization, and slow energy absorption in periodically driven many-body systems, *Reviews of Modern Physics* **89**, 011001 (2017).
- [14] D. J. Luitz, N. Laflorencie, and F. Alet, Many-body localization edge in the random-field heisenberg chain, *Physical Review B* **91**, 081103 (2015).
- [15] J. H. Bardarson, F. Pollmann, and J. E. Moore, Unbounded growth of entanglement in models of many-body localization, *Physical review letters* **109**, 017202 (2012).
- [16] M. Žnidarič, T. c. v. Prosen, and P. Prelovšek, Many-body localization in the heisenberg xxz magnet in a random field, *Phys. Rev. B* **77**, 064426 (2008).
- [17] Y. Li, X. Chen, and M. P. Fisher, Quantum zeno effect and the many-body entanglement transition, *Physical Review B* **98**, 205136 (2018).
- [18] B. Skinner, J. Ruhman, and A. Nahum, Measurement-induced phase transitions in the dynamics of entanglement, *Physical Review X* **9**, 031009 (2019).
- [19] E. Altman, R. Vasseur, and A. C. Potter, Statistical mechanics of quantum error correction and the measurement-induced transition, *Phys. Rev. B* **104**, 134204 (2021).
- [20] A. Nahum, S. Roy, B. Skinner, and J. Ruhman, Measurement and entanglement phase transitions in all-to-all quantum circuits, on quantum trees, and in landau-ginzburg theory, *PRX Quantum* **2**, 010352 (2021).
- [21] M. Ippoliti, M. J. Gullans, S. Gopalakrishnan, D. A. Huse, and V. Khemani, Entanglement phase transitions in measurement-only dynamics, *Physical Review X* **11**, 011030 (2021).
- [22] O. Lunt and A. Pal, Measurement-induced entanglement transitions in many-body localized systems, *Phys. Rev. Res.* **2**, 043072 (2020).
- [23] K. Yamamoto and R. Hamazaki, Localization properties in disordered quantum many-body dynamics under continuous measurement, *Phys. Rev. B* **107**, L220201 (2023).
- [24] G. De Tomasi and I. M. Khaymovich, Stable many-body localization under random continuous measurements in the no-click limit, *Phys. Rev. B* **109**, 174205 (2024).
- [25] A. Weiße, G. Wellein, A. Alvermann, and H. Fehske, The kernel polynomial method, *Rev. Mod. Phys.* **78**, 275 (2006).
- [26] J. Smith, A. Lee, P. Richerme, B. Neyenhuis, P. W. Hess, P. Hauke, M. Heyl, D. A. Huse, and C. Monroe, Many-body localization in a quantum simulator with programmable random disorder, *Nature Physics* **12**, 907 (2016).
- [27] J.-y. Choi, S. Hild, J. Zeiher, P. Schauß, A. Rubio-Abadal, T. Yefsah, V. Khemani, D. A. Huse, I. Bloch, and C. Gross, Exploring the many-body localization transition in two dimensions, *Science* **352**, 1547 (2016).
- [28] G. Kucsko, S. Choi, J. Choi, P. C. Maurer, H. Zhou, R. Landig, H. Sumiya, S. Onoda, J. Isoya, F. Jelezko, et al., Critical thermalization of a disordered dipolar spin system in diamond, *Physical review letters* **121**, 023601 (2018).
- [29] M. Gong, G. D. de Moraes Neto, C. Zha, Y. Wu, H. Rong, Y. Ye, S. Li, Q. Zhu, S. Wang, Y. Zhao, et al., Experimental characterization of the quantum many-body localization transition, *Physical Review Research* **3**, 033043 (2021).
- [30] P. Roushan, C. Neill, J. Tangpanitanon, V. M. Bastidas, A. Megrant, R. Barends, Y. Chen, Z. Chen, B. Chiaro, A. Dunsworth, et al., Spectroscopic signatures of localization with interacting photons in superconducting qubits, *Science* **358**, 1175 (2017).
- [31] B. Chiaro, B. Foxen, M. McEwen, and J. Martinis, Growth and preservation of entanglement in a many-body localized system, *Bulletin of the American Physical Society* **65** (2020).
- [32] T. Kohlert, S. Scherg, X. Li, H. P. Lüschen, S. Das Sarma, I. Bloch, and M. Aidelsburger, Observation of many-body localization in a one-dimensional system with a single-particle mobility edge, *Physical review letters* **122**, 170403 (2019).
- [33] D. Zhu, S. Johri, N. Nguyen, C. H. Alderete, K. Landsman, N. Linke, C. Monroe, and A. Matsuura, Probing many-body localization on a noisy quantum computer, *Physical Review A* **103**, 032606 (2021).
- [34] M. Schreiber, S. S. Hodgman, P. Bordia, H. P. Lüschen, M. H. Fischer, R. Vosk, E. Altman, U. Schneider, and I. Bloch, Observation of many-body localization of interacting fermions in a quasirandom optical lattice, *Science* **349**, 842 (2015).
- [35] P. Bordia, H. Lüschen, S. Scherg, S. Gopalakrishnan, M. Knap, U. Schneider, and I. Bloch, Probing slow relaxation and many-body localization in two-dimensional quasiperiodic systems, *Physical Review X* **7**, 041047 (2017).
- [36] C. Noel, P. Niroula, D. Zhu, A. Risinger, L. Egan, D. Biswas, M. Cetina, A. V. Gorshkov, M. J. Gullans, D. A. Huse, et al., Measurement-induced quantum phases realized in a trapped-ion quantum computer, *Nature Physics* **18**, 760 (2022).
- [37] J. M. Koh, S.-N. Sun, M. Motta, and A. J. Minnich, Experimental realization of a measurement-induced entanglement phase transition on a superconducting quantum processor, *arXiv preprint arXiv:2203.04338* (2022).
- [38] Measurement-induced entanglement and teleportation on a noisy quantum processor, *Nature* **622**, 481 (2023).
- [39] U. Agrawal, J. Lopez-Piqueres, R. Vasseur, S. Gopalakrishnan, and A. C. Potter, Observing quantum measurement collapse as a learnability phase transition, *Physical Review X* **14**, 041012 (2024).
- [40] X. Feng, J. Côté, S. Kourtis, and B. Skinner, Postselection-free experimental observation of the measurement-induced phase transition in circuits with universal gates, *arXiv preprint arXiv:2502.01735* (2025).
- [41] D. Sels, Bath-induced delocalization in interacting disordered spin chains, *Phys. Rev. B* **106**, L020202 (2022).
- [42] A. Morningstar, L. Colmenarez, V. Khemani, D. J. Luitz, and D. A. Huse, Avalanches and many-body resonances in many-body localized systems, *Phys. Rev. B* **105**, 174205 (2022).
- [43] M. Serbyn, Z. Papić, and D. A. Abanin, Local conservation laws and the structure of the many-body localized states, *Physical review letters* **111**, 127201 (2013).
- [44] D. A. Huse, R. Nandkishore, and V. Oganesyan, Phenomenology of fully many-body-localized systems, *Physical Review B* **90**, 174202 (2014).
- [45] M. Serbyn, Z. Papić, and D. A. Abanin, Universal slow growth of entanglement in interacting strongly disordered systems, *Phys. Rev. Lett.* **110**, 260601 (2013).
- [46] A. Zabalo, M. J. Gullans, J. H. Wilson, S. Gopalakrishnan, D. A. Huse, and J. H. Pixley, Critical properties of

the measurement-induced transition in random quantum circuits, *Phys. Rev. B* **101**, 060301 (2020).

- [47] Y. Bao, S. Choi, and E. Altman, Theory of the phase transition in random quantum circuits, *Physical Review B* **101**, 104301 (2020).
- [48] M. J. Gullans and D. A. Huse, Dynamical purification transition induced by measurements, *Physical Review Letters* **125**, 070606 (2020).
- [49] A. Chandran, I. H. Kim, G. Vidal, and D. A. Abanin, Constructing local integrals of motion in the many-body localized phase, *Physical Review B* **91**, 085425 (2015).
- [50] H. Fehske, R. Schneider, and A. Weiss, *Computational many-particle physics*, Vol. 739 (Springer, 2007).

END MATTER

Unitary time evolution

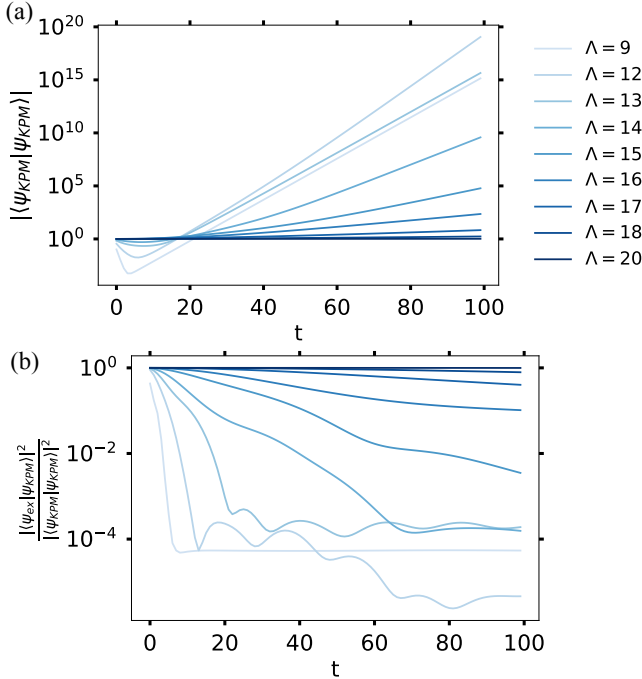


FIG. 5: We evolve the state $|\psi_0\rangle = \otimes_{i=1}^L |\uparrow\rangle$ with the Hamiltonian (1) for system size $L = 8$ and disorder strength $W = 5$. (a) Norm of $|\psi_{\text{KPM}}\rangle$ as a function of time for different truncation orders Λ . (b) Fidelity of the KPM wavefunction $|\psi_{\text{KPM}}\rangle$ for different Λ as compared with the exact time evolved state $|\psi_{\text{ex}}\rangle$.

Instead of diagonalizing the microscopic Hamiltonian, which becomes intractable for large systems, we approximate the exponential $U = e^{-iH\delta t}$ using the kernel polynomial method (KPM) following Ref. [50]. This method utilizes Chebyshev polynomials $T_n(x)$ defined on the interval $x \in [-1, 1]$. Therefore, we first rescale the Hamil-

tonian H so that its spectrum lies within this interval:

$$\tilde{H} = \frac{H - b}{a}, \quad a = \frac{E_{\text{max}} - E_{\text{min}}}{2}, \quad b = \frac{E_{\text{max}} + E_{\text{min}}}{2}, \quad (8)$$

where E_{min} and E_{max} denote the minimum and maximum eigenvalues of H .

With this rescaling, the time evolution operator can be written as

$$U(t) = e^{-iHt} = e^{-ibt} e^{-iat\tilde{H}}. \quad (9)$$

The global phase factor e^{-ibt} is exact, while the non-trivial part $e^{-iat\tilde{H}}$ is expanded in terms of Chebyshev polynomials to an order Λ :

$$e^{-iat\tilde{H}} \approx J_0(at)I + 2 \sum_{n=1}^{\Lambda} (-i)^n J_n(at) T_n(\tilde{H}), \quad (10)$$

where J_n are Bessel functions of the first kind.

Chebyshev polynomials are generated recursively according to

$$T_0(x) = 1, \quad T_1(x) = x, \quad T_{n+1}(x) = 2xT_n(x) - T_{n-1}(x). \quad (11)$$

Thus, for any initial state $|\psi\rangle$, the propagated state at time t can be approximated as

$$|\psi(t)\rangle \approx e^{-ibt} \left[J_0(at) |\phi_0\rangle + 2 \sum_{n=1}^{\Lambda} (-i)^n J_n(at) |\phi_n\rangle \right], \quad (12)$$

with the vectors $\{|\phi_n\rangle\}$ defined recursively by

$$|\phi_0\rangle = |\psi\rangle, \quad |\phi_1\rangle = \tilde{H} |\psi\rangle, \quad |\phi_{n+1}\rangle = 2\tilde{H} |\phi_n\rangle - |\phi_{n-1}\rangle. \quad (13)$$

This expansion reduces the problem to a sequence of sparse matrix-vector multiplications, avoiding the direct exponentiation of a large $2^N \times 2^N$ matrix.

We gauge the accuracy of the Chebyshev expansion through the fidelity of the KPM. We compare the time-evolved state obtained from exact propagation, $|\psi_{\text{ex}}(t)\rangle = e^{-iHt} |\psi_0\rangle$ with the one obtained from the Chebyshev expansion, $|\psi_{\text{KPM}}(t)\rangle = U_{\text{KPM}} |\psi_{\text{KPM}}(t-1)\rangle$ by evaluating the overlap $F(t) = \langle \psi_{\text{ex}}(t) | \psi_{\text{KPM}}(t) \rangle$. The two methods agree when $\Lambda \gtrsim 20$ as shown in Fig. 5. In the calculations presented in the main text, we fix $\Lambda = 400$, for which the results are indistinguishable from those obtained by exact time evolution.

Level spacing ratio of the microscopic model

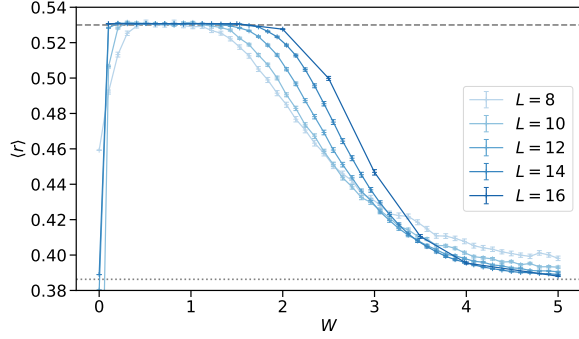


FIG. 6: Average level-spacing ratio $\langle r \rangle$ for the Hamiltonian (1) as a function of disorder strength W for several system sizes L . The dashed gray line indicates the Gaussian orthogonal ensemble value $\langle r \rangle \approx 0.53$, while the dotted gray line marks the Poisson value $\langle r \rangle = 2 \ln 2 - 1$.

To diagnose the many-body localization transition, we study the spectral statistics of the microscopic Hamiltonian (1). First, we obtain the ordered eigenvalues

$$E_0 < E_1 < E_2 < \dots < E_{2^L-1}, \quad (14)$$

by exact diagonalization. We define the consecutive level spacings

$$\delta_i = E_{i+1} - E_i, \quad (15)$$

and the level spacing ratios

$$r_i = \frac{\min(\delta_i, \delta_{i-1})}{\max(\delta_i, \delta_{i-1})}, \quad i = 1, 2, \dots, 2^L - 2. \quad (16)$$

The average value $\langle r \rangle$ over disorder realizations (500 samples) and a chosen energy window (middle 60%) serves as a sensitive probe of localization in a finite size system. For $W = 0$, the model is integrable and hence level spacings follow Poisson distribution with the average ratio $\langle r \rangle \sim 0.39$, see Fig. 6. As W increases, the system becomes chaotic and hence level spacings conform to the Gaussian orthogonal ensemble (GOE) with average ratio $\langle r \rangle \sim 0.53$. As W increases further, the level spacing distribution reverts back to Poisson, indicating that the system is now in an MBL phase. From the crossing of the curves for various L , we infer that a transition to the localized phase occurs at the critical value of $W_c \gtrsim 3.2$.

Note, however, that while this computation performed for a finite system seems to indicate a transition at a small value of $W_c = 3.2$, more careful studies have revealed that this is in fact an extended prethermal crossover regime, and true many-body localization, if it occurs, will take place at a much larger disorder strength.

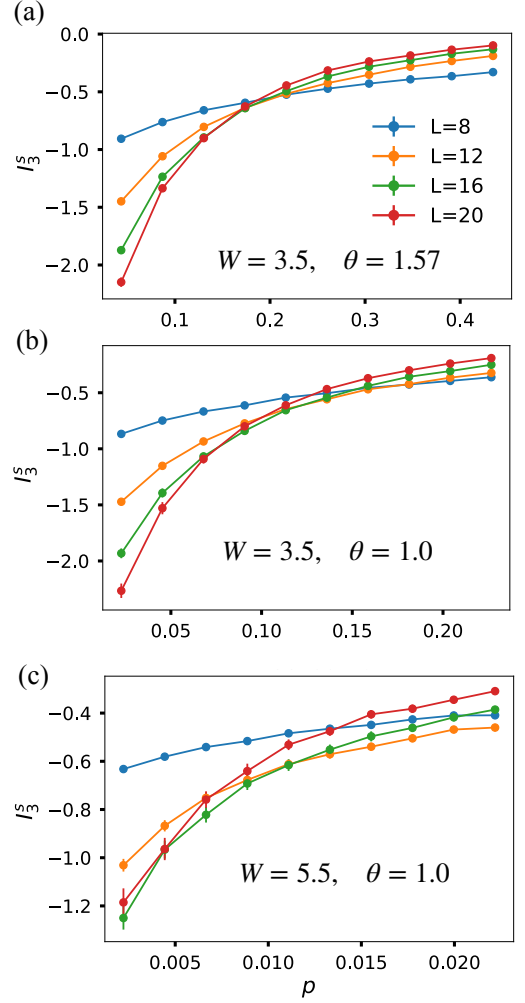


FIG. 7: Three examples of crossings of plots of the tripartite mutual information I_3^s vs. the measurement rate p . Observe that finite-size effects become stronger as the disorder strength W increases or the measurement angle θ decreases. (a) $W = 3.5$ and $\theta = 1.57$. Finite size effects are negligible. (b) $W = 3.5$ and $\theta = 1.0$. The $L = 8$ plot is not crossing at the same point as the plots for other L . (c) $W = 5.5$ and $\theta = 1.0$. Finite size effects are strongest and there is no clearly discernible crossing point.

Critical measurement rate

To evaluate the critical measurement rate p_c for the microscopic model, we calculate the averaged tripartite mutual information I_3 as discussed in the main text. In Fig. 7, we show three representative examples of the data crossings for I_3 . As $\theta \rightarrow 0$ and $W \rightarrow \infty$, the critical measurement rate $p_c \rightarrow 0$ and the finite-size effects become stronger. As the finite size effects are very large for $L = 8$, we extrapolate the critical measurement rate from $L = 12, 16$, and 20 using the best fit to the scaling

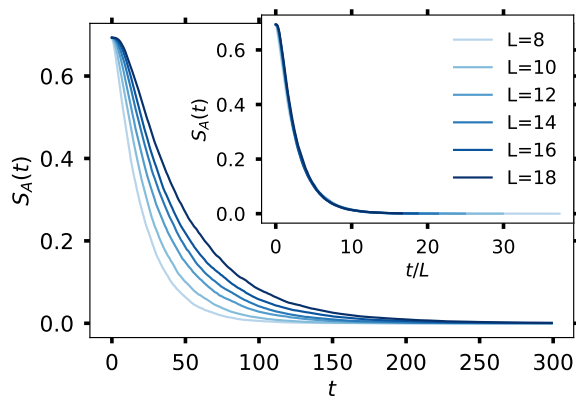


FIG. 8: Average ancilla entropy $S_A(t)$ for the l -bit model at the critical measurement rate $p = p_c$. The inset shows that plots for different system sizes L collapse onto a single curve $S_A(t/L)$ indicating that the dynamical exponent $z = 1$.

function $I_3(t \rightarrow \infty) \sim f((p - p_c)L^{1/\nu})$. In cases such as Fig. 7(c), when the crossing is difficult to discern, we

marked the corresponding p_c with a hollow dot in Fig. 3.

Ancilla

To determine the dynamical exponent z at criticality, $p = p_c$, we calculate the average ancilla entropy $S_A(t) = [\bar{S}_A^{\{\eta, m_i(t)\}}(t)]$ for the l -bit model coupled to an ancilla A . Fig. 8 shows that the ancilla entropy obeys the scaling $S_A(t, L) = S_A(t/L)$, where L is the system size. We therefore conclude that $z = 1$.

To calculate S_A numerically, we start from an initial state $\frac{1}{\sqrt{2}}(|0\rangle_A \otimes |\phi_1\rangle + |1\rangle_A \otimes |\phi_2\rangle)$, with $\langle \phi_1 | \phi_2 \rangle = 0$. Here A stands for the ancilla and $|\phi\rangle$ is the state of the system. The system is evolved under the protocol discussed in the main text. At each time step, we calculate the entanglement entropy between the ancilla and the system $S_A^{\{\eta, m_i(t)\}}(t) = -\rho_A \ln \rho_A$. In Fig. 8, we show the ancilla entropy $S_A(t) = [\bar{S}_A^{\{\eta, m_i(t)\}}(t)]$ averaged over 2000 quantum trajectories and realizations of the random variables η .